Journal of Energy Storage 60 (2023) 106660

Contents lists available at ScienceDirect

Journal of Energy Storage

journal homepage: www.elsevier.com/locate/est

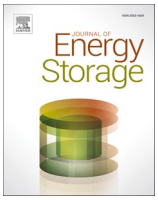

Research papers

Energy harvesting and storage with ceramic piezoelectric transducers coupled with an ionic liquid-based supercapacitor

Giacomo Selleri [a,*], Federico Poli [b,*], Riccardo Neri [a], Leonardo Gasperini [a], Chiara Gualandi [b], Francesca Soavi [b], Davide Fabiani [a]

[a] Department of Electrical, Electronic, and Information Engineering, University of Bologna, Viale Risorgimento 2, 40136 Bologna, Italy
[b] Department of Chemistry "Giacomo Ciamician" and INSTM UdR of Bologna, University of Bologna, via Selmi 2, 40126 Bologna, Italy

ARTICLE INFO

Keywords:
Energy harvesting
Piezoelectricity
Supercapacitor
Self-charging
Wearable electronics

ABSTRACT

One of the main issues of wearable electronic devices regards their power supply and autonomy. The exploitation of mechanical energy from body motion and vibrations can be realized by using piezoelectric materials coupled with a proper energy storage device. To this aim, Self-Powered Supercapacitors (SPSCs) have been investigated over the last decades, either as internally integrated SPSC (iSPSC), where the piezoelectric element of the device is used as Super Capacitor (SC) separator, or via an external integration (eSPSC), where the piezoelectric unit and the SC are connected by a bridge rectifier. In this paper, an eSPSC power supply is developed by integrating a stuck of commercial ceramic piezoelectric disks and an ionic liquid-based micro-SC. In detail, a stack of 15 commercial lead zirconate titanate (PZT) disks is used as the energy harvesting unit and mechanically stressed by a compressive force of 85 N at 2 Hz. The piezoelectric output successfully charged the 22 mF supercapacitor up to 3.1 V after 2 h of test, achieving a stored energy value equal to 110 mJ. The proposed integrated system outperforms the state-of-the-art SPSC assembled with micro-SC (both iSPSC and eSPSC). The use of the two different units (piezo-energy harvesting unit and micro-SC energy storage unit) allows an independent sizing and tuning of the supercapacitor according to the output current of the piezoelectric unit.

1. Introduction

The use of electronic devices is tremendously increasing for various applications, ranging from the consumer market to Internet of Things (IoT) and wearable devices. Over the years, the energy efficiency of electronic devices has significantly improved, resulting in a lower energy requirement. However, sensors, flashlights, and phones still rely on batteries for their power supply, leading to issues regarding their replacement and recharging. Power autonomy is especially required in the cases of remote-located sensors or implantable bio-medical devices. In this context, ambient energy harvesters are attracting enormous interest. The possibilities to significantly increase the duration of the in-use device's batteries or to replace them by harvesting enough energy from the surrounding environment, represent an interesting branch of research. The most common sources of energy from the environment are light, heat, wind, electromagnetic Radio Frequency (RF), and mechanical energies [1,2]. Energy harvesting from body motions or vibrations, such as walking or breathing, by piezoelectric systems, provides an excellent approach to power wearable devices [2]. The piezoelectric transducing mechanism paves the way for a variety of energy harvesting technologies which do not depend on environmental conditions and the weather, differently from other non-programmable sources such as wind, thermal and solar energy. For instance, they could be installed on a system that is frequently subjected to mechanical stress, such as bridges or highways. Other piezoelectric-based systems have been designed for energy harvesting from mechanical stimuli, such as the kinetic energy of highway traffic [3]. The strain-induced polarization of piezoelectric materials generates an electric voltage as the result of the mechanical deformation of their crystal lattice. A wide variety of piezoelectric nanogenerators (PENGs) has been investigated, relying on different piezoelectric materials and nanostructures [4]. Lead zirconate titanate (PZT) stands out for its piezoelectric performance. Numerous kinds of devices based on PZT disks were fabricated in different designs, like cymbals geometries [5–6] or cantilevers. Motter et al. demonstrated the feasibility of vibrational energy harvesting based on a piezoelectric cantilever beam to light a LED or to monitor the state of charge of a

* Corresponding authors.
E-mail addresses: giacomo.selleri2@unibo.it (G. Selleri), federico.poli8@unibo.it (F. Poli).

https://doi.org/10.1016/j.est.2023.106660
Received 10 November 2022; Received in revised form 27 December 2022; Accepted 8 January 2023
Available online 14 January 2023

storage system, like a battery or a capacitor [7].

Power generation and demand are often mismatched both in time and place. Full exploitation of PENGs requires that the harvested energy is readily available at high-quality on demand. However, most of energy harvesters typically provide intermittent and low power and voltage outputs, so their integration with energy storage units, like batteries and, mainly, supercapacitors (SCs), is mandatory [8]. Specifically, the storage unit has to be tailored, both to meet the device design requirements (flexibility, thickness, size) and the electric behavior of the harvester. While SCs are outperformed by batteries in terms of energy density, they exhibit superior cycling stability and power performance, which is of paramount importance for applications having frequent high peak-to-average power demand. This is related to their capability to electrostatically store/deliver charges in a relatively short time. In addition, unlike batteries that store energy at given cell voltages set by the electrode Faradaic processes, electrical double-layer capacitors (EDLCs) store energy electrostatically within a wide working voltage range, which is limited only by the electrochemical stability of the electrolyte. This dynamic response of EDLCs enables their combination with a wide range of energy harvesters including those operating at low voltage like PENGs [8].

The typical configuration of SCs consists of two high-surface-area carbon electrodes, separated by the electrolyte (either organic or aqueous) and the separator. Such a simple design stack has been proposed by exploiting many architectures, from traditional bulky and rigid SCs (coin, button, cylindrical and prismatic cells) to flexible and fiber-shaped SCs [9]. The research activity is currently dedicated to developing lightweight, foldable, bendable, and even wearable SPs. However, the greatest challenge in achieving flexible SPs with excellent electrochemical performance and mechanical properties is the selection and manufacturing of flexible electrodes coupled with proper electrolytes [10]. In addition, the growing demand for energy-autonomous electronic components makes urgent the implementation of sustainable SC materials and manufacturing processes. Indeed, today SCs electrodes are produced by casting toxic suspensions of carbon in poly(vinylidene difluoride) (PVDF)-*N*-methyl-2-pyrrolidone (NMP). Water-soluble polymers, like alginate, or pullulan, have been demonstrated to be a valuable green alternative to PVdF binder, both for IL-based SCs and lithium batteries [11–14]. Concerning electrolytes, ionic liquids (ILs) for their high ionic conductivity, wide electrochemical stability, low vapor pressure, and non-flammability are emerging as a safer alternative to conventional organic electrolytes for flexible, thin SCs operating at 3 V and above [15–16]. ILs have also been reported to provide SCs with lower leakage currents and self-discharge than conventional organic electrolytes. N-butyl-*N*-methylpyrrolidinium bis(trifluoromethanesulfonyl)imide (PYR14TFSI)-based SCs emerged for their negligible leakage currents and self-discharge up to 3.2 V [17]. This is important because of the integration of SCs with energy harvesters operating at low current regimes, like PENGs. Indeed, SCs current regimes (ca. 100 mA F^{-1}) are typically higher than those generated by PENGs (hundreds of μA) and that, in turn, can be in the order of magnitude of SCs leakage currents (<1 μA F^{-1}, as the suggested target for commercial SCs [17–19]). In order to effectively charge the SCs, the charging currents provided by the harvester should be higher than the leakage ones. Hence, in piezo-supercapacitor systems, the SCs should be properly sized, namely, miniaturized, to meet such requirements.

Over the last decade, two main PENG-SC integration approaches have been proposed for the design of the so-called self-powered supercapacitors (SPSCs): i) PENG-SC internal (monolithic) integration (iSPSC), where the PENG film is used as SC separator [20], or ii) PENG-SC external integration (eSPSC), where the two separate PENG and SC units, are connected by a bridge rectifier that converts the alternate current from the energy harvester into direct current for charging SCs [21–22]. Table 1 lists the performance, in terms of capacitance (C), charging time and voltage reached during charge (V_{ch}) of iSPSCs assembled with piezoelectric membranes acting both as separator and nanogenerator. The table also reports the maximum energy (E_{max}) that can be stored, calculated by Eq. (1):

$$E_{max} = \frac{1}{2} C V_{ch}^2 \tag{1}$$

PVDF (or its piezoelectric copolymer PVDF-TrFE) is widely used for the fabrication of SPSCs (Table 1). Indeed, PVDF simultaneously features good piezoelectric performances (d_{33}=20–25 pC N^{-1}), high flexibility and easy-processability (nanofibers, foams, films), which are advantageous characteristics for the development of wearable and flexible devices. However, PVdF membranes are often processed using the toxic NMP solvent, which negatively impacts on system production sustainability. In addition, the external frame of SPSCs (electrodes and sealing layers) might reduce or smooth the load transferred to the piezo-separator and, in the case of high mechanical impacts, structural damages could occur in the device. SCs with higher self-powering efficiencies could be produced by using ceramic piezoelectric materials such as PZT, which typically presents piezoelectric strain coefficients d_{33} one order of magnitude higher than the piezo-polymers ones (d_{33}=200–600 pC N^{-1}). However, PZTs are brittle and fragile, which hampers their use as separators of SPSCs.

The external connection of two separated PENG and SC units in eSPSC represents a straightforward solution. Indeed, the eSPSC architecture enables to separately size the SC and the PENG allowing improved system efficiency. It has been demonstrated both with flexible, or micro-SCs, eventually patterned on the PENG stack, and commercial SCs (button, cylindrical). Some examples of eSPSC are listed in Table 2. A comparison of the data summarized in Tables 1 and 2 clearly shows that the external connections enable achieving higher system voltages if the two systems (PENG-SC) are coupled with appropriate circuits. For instance, the use of bridge rectifiers allows reversing the negative polarity peaks of the piezoelectric output, thus enhancing the energy conversion efficiency of the system. Indeed, the energy storage performance of eSPSC can be more than one order of magnitude higher than that of the monolithically integrated iSPSC depending on the SC size. In turn, this results in longer charging times (minutes-hours vs seconds-minutes).

In this work, a piezoelectric stack of 15-PZT disks is used as the energy harvesting source to charge an IL-pullulan-based micro-SC. The piezoelectric performances of the energy harvesting unit and the coupling circuit with the SC are studied to estimate the capability of the piezo-transducers to effectively charge the SC.

Table 1
Performance of self-powered iSPSC with SC piezoelectric separator: capacitance, charging time, and voltage and stored maximum energy (from Eq. (1)) generated at given mechanical stimulus.

Piezoelectric separator	SC capacitance	Charging time	Charging voltage V_{ch}	Mechanical stimuli	E_{max}	Ref
PVDF-ZnO film	257 mF g^{-1}	360 s	0.350 V	Palm impact force at 9.8 N	15 mJ g^{-1}	[23]
PVDF film	35.8 mF cm^{-2}	50 s	0.090 V	Compressive force @ 4.5 Hz	145 μJ cm^{-2}	[24]
PVDF-TrFE film	23.1 μF cm^{-2}	17 s	0.450 V	90° bending	2.3 μJ cm^{-2}	[25]
Porous PVDF-TrFE foam	95 μ F cm^{-2}	10 s	0.320 V	Compressive force 70 N at 5 Hz	4.8 μJ cm^{-2}	[26]
PVDF-TrFE film	50 F g^{-1}	20 s	0.500 V	Compressive force 12,2 N at 2.5 Hz	6.2 J g^{-1}	[27]
PVDF-TrFE nanofibers	3.6 mF cm^{-2}	250 s	0.314 V	Compressive force 20 N	177 μJ cm^{-2}	[28]
Bio-piezoelectric separator (fish swim bladder)	330 mF cm^{-2}	80 s	0,280 V	Human hand impact of 16.4 N @ 1.65 Hz	13 mJ cm^{-2}	[29]

Table 2
List of eSPSCs systems: SC capacitance and type, charging time and voltage and stored maximum energy (from Eq. (1)) generated at given mechanical stimulus.

Piezo-energy harvesting unit	SC capacitance	Charging time	Charging voltage	Mechanical stimuli	Stored energy	Ref
PVDF film	470 μF	40 s	1.00 V	Bending @ 50 Hz	300 μJ	[19]
PVDF nanofibers	22.6 mF cm^{-2} (patterned)	180 s	0.289 V	Continuous palm impacting	0.94 mJ cm^{-2}	[30]
PZT film	22 mF (patterned)	16 h	2 V	Bending at 1.7 Hz	44 mJ	[31]
PZT cantilever	8 mF (11 cells) (flexible)	11 h	2.6 V	Bending at 3 Hz	27 mJ	[32]
12 × PZT disk	250 mF	41 min	2.7 V	Compression @ 2.8 Hz	0.9 J	[33]
	1 F button cell (commercial)	5 h			3.6 J	
PZT stack	6.6 mF	1 s	4.5 V	12.5 N compression @ 1790 Hz	66.2 mJ	[34]
PZT disk	330 mF button cell (commercial)	12 h	2.5 V	Bending @ 2.42 Hz	1 J	[35]
4 × PZT bimorph	1 mF button cell (>2 cells, commercial)	15 s	8 V	Bending @ 47–57 Hz	32 mJ	[36]

With the final purpose to design an energy harvesting system for low-frequency applications and to tailor a proper sizing of the proposed SC with reference to the piezoelectric output current, the experiments were conducted with regular compressive tests at 2 Hz. This work represents the proof of concept before considering irregular movements, which are typical of environmental mechanical movements. The use of an eSCSP system allowed to separately characterize both the piezo-generator and the supercapacitor, in order to properly tune the piezoelectric current with a specifically sized supercapacitor and achieve high voltages without leakages, differently from a commercial capacitor.

2. Materials and methods

2.1. Piezoelectric transducer

The piezoelectric transducer used to build the energy harvesting unit is a ceramic PZT disk (7BB-20-3 Murata) of 100 μm thickness and a diameter of 14 mm, as shown in Fig. 1. It was covered on one side by a silver electrode with a diameter of 12.5 mm and on the other side by a brass layer with a thickness of 120 μm and a diameter of about 20 mm. Before building the energy harvesting unit - which consists of 15 ceramic disks - the piezoelectric performances and the dielectric properties were measured on the single piezoelectric transducer, and the experimental apparatus, as well as the measurements conditions, are reported and discussed in the following sections.

2.1.1. Piezoelectric coefficient measurements

The piezoelectric strain coefficient d_{33} of the disk was measured by using both a home-made setup and a piezometer (d_{33} PiezoMeter System, Piezotest, Singapore, www.piezotest.com). The homemade measuring apparatus consists of a linear motor (LinMot) equipped with a 300 N (Model 1042, Single point load cells, Tedea-Huntleigh). The PZT disk was placed over the load cell and was compressed between a flat plate and a 1.4 cm diameter cylindric indenter, as shown in Fig. 2a. The flat support and the indenter were made of brass and connected to an electrometer (Keithley 6517B, input impedance >200 TΩ) to measure the generated charges. The load cell signal and the piezoelectric output were thus simultaneously displayed on a digital oscilloscope (Tektronix DPO 5034B, digital phosphoric oscilloscope), as schematically represented in Fig. 1. The piezoelectric strain coefficient d_{33} of the single PZT disk can be calculated as the ratio of the peak-to-peak charge value collected by the electrodes and the peak-to-peak value of the applied force.

For the sake of the reliability of the measurement, the piezoelectric strain coefficient d_{33} of the PZT disk was also evaluated through the piezometer. The d_{33} coefficient measurement was performed by stressing the samples with a compressing sinusoidal force of 0.25 N at 100 Hz frequency. The piezoelectric voltage coefficient g_{33} has been calculated according to Eq. (2):

$$g_{33} = \frac{d_{33}}{\varepsilon_r \bullet \varepsilon_0} \tag{2}$$

where ε_r is the relative permittivity of the PZT disk and ε_0 is the vacuum permittivity (8.85 × 10^{-12} F m^{-1}).

2.1.2. Dielectric measurements

The capacitance, permittivity, and resistance of the PZT disk have been measured employing the Novocontrol Alpha Dielectric Analyzer v2.2. It is based on a voltage amplifier for the application of variable frequency electric fields and a measuring cell comprising the high voltage and ground electrodes. Measurements of the capacitance, resistance, and permittivity have been carried out by applying an oscillating electric field in the frequency range between 10^{-1} and 10^{4} Hz.

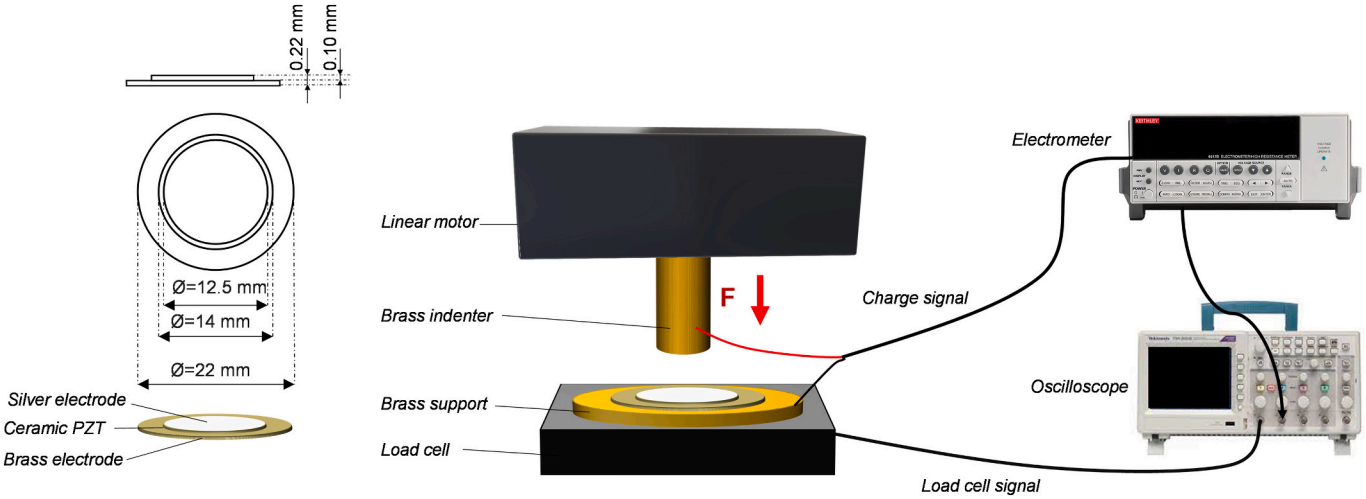

Fig. 1. PZT commercial disk dimensions and acquisition circuit representation.

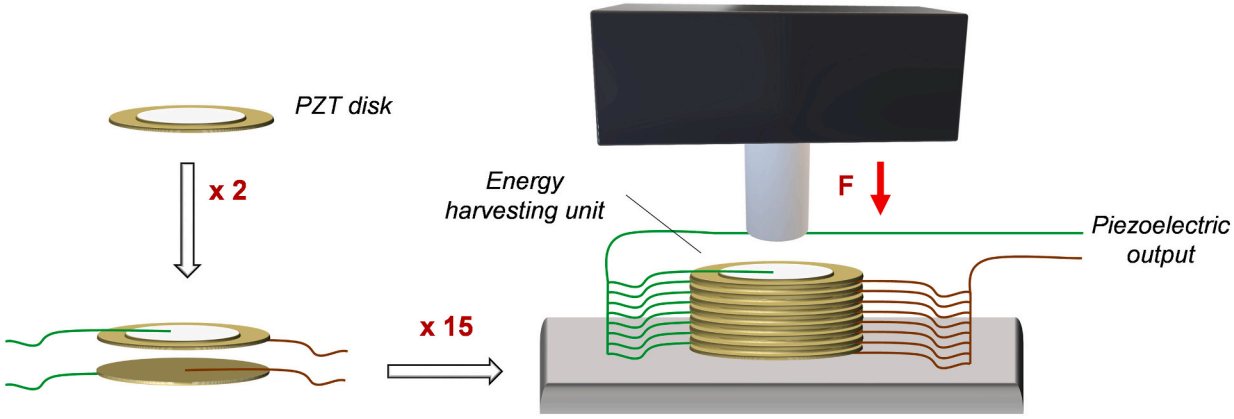

Fig. 2. Energy harvesting unit and schematic representation of the 15 PZT commercial disks disposition.

2.2. Energy harvesting unit

The energy harvesting unit consists of multiple piezoelectric transducers parallelly connected and placed on top of each other. The polarity of the piezoelectric output was preserved by connecting the silver electrodes of each PZT disk with a common copper tape and connecting the brass sheets to a second copper tape disposed on the opposite side of the device, as schematically reported in Fig. 2. This configuration presents N + 1 outcoming electrodes for N piezoelectric elements, thus limiting the whole size of the system and the number of copper tape-electrodes. Following the explained building strategy, 15 piezoelectric disks were stacked together to have a considerable electrical energy output sufficient for the supercapacitor charging. The whole piezoelectric energy harvesting generator was encapsulated with an insulating tape and placed over a stiff insulating base in such a way that the force applied on the first disk is equally transferred to the underlying ones as well. Before coupling with the supercapacitor, the energy harvesting unit was characterized in terms of output voltage and generated current, by connecting the piezoelectric output to the electrometer and the ammeter, respectively. The short-circuit current and open circuit voltage were simultaneously acquired in response to a 2 Hz compressive sinusoidal load oscillating between 0 and 85 N.

2.3. Supercapacitor: manufacturing and testing

SCs were assembled from two carbon composite electrodes alienated by a Whatman GF fiber glass separator. The electrolyte was N-butyl-*N*-methylpyrrolidinium bis(trifluoromethanesulfonyl)imide (PYR14TFSI, purity >99.9 %, Solvionic). Electrodes were prepared using the activated carbon YP-80F (Kuraray, 2364 $m^2\ g^{-1}$) and a mixture of pullulan-glycerol (1:1 in weight) as the binder. Specifically, electrode weight composition was 70%wt activated carbon YP-80F, 20%wt Pullulan-Glycerol binder, and 10%wt SuperC45 carbon. The composite powders were dispersed in water, homogenized by stirring and cast on aluminum current collectors with a minicoater (MINICOATEP MODEL: MC20 Hohsen), pressed and dried overnight at room temperature (Büchi glass oven B-585). The final composite loading was 1.3 mg cm^{-2}. Finally, the electrodes and the separator were stacked in a plastic bag, filled with the IL, and sealed in a dry box (Ar atmosphere, H_2O, and O_2 < 1 ppm). Before integration with the piezoelectric source, the SC was tested by galvanostatic charge/discharge cycles with potential limitation (GCPL) at room temperature using a BioLogic VSP multichannel potentiostat/galvanostat. The cell capacitance was calculated from the reciprocal of the slope of the discharge curve (dV/dt) of the GCD plots collected at 2-electrode, using Eq. (3):

$$C = I\frac{dt}{dV} \tag{3}$$

where I is the discharge current.

The SC equivalent series resistance (ESR) was evaluated by the ohmic drop at the beginning of discharge by Eq. (4):

$$ESR = \frac{1}{2}\frac{\Delta V}{I} \tag{4}$$

C and ESR were then used to calculate the maximum energy (E_{max}, in Wh) and power (P_{max}) performance of the SC by Eqs. (1) and (5):

$$P_{max} = \frac{1}{4}\frac{V_{max}^2}{ESR} \tag{5}$$

where V_{max} is the charge cut-off voltage (3 V).

The maximum current deliverable by the SC (through an external load having the same value of ESR) is calculated through Eq. (6):

$$I_{max} = \frac{V_{max}}{2ESR} \tag{6}$$

2.4. Piezoelectric energy harvester – supercapacitor coupling

Fig. 3 reports the piezoelectric generator-supercapacitor coupling circuit. This includes a part dedicated to the charging process of the supercapacitor and a part where the stored energy is transferred to the resistive load R_{load} for the discharging process. The Single Pole Double Throw (SPDT) relay swaps between the charging phase of the circuit (COM-NC connection) and the discharging phase (COM-NO connection). During the charging phase, the piezoelectric unit is mechanically compressed by a sinusoidal load of 85 N at 2 Hz by the linear motor of Fig. 2. The alternating piezoelectric output passes through the full-wave diode bridge rectifier and charges the supercapacitor. The bridge rectifier is composed of four Small Signal Schottky Diode (SD-103-A, Vishay) which feature low forward voltage drop (370 mV for 20 mA current). The current is measured in the ammeter (A in Fig. 3) while a voltmeter measures the voltage (V in Fig. 3) across the supercapacitor.

The charging process setup of the SC is observable in Fig. 4, where the piezoelectric energy harvesting unit is compressed by the linear motor and the output current flows through the bridge rectifier before to reach the SC.

3. Results and discussion

3.1. Piezoelectric generator

The piezoelectric response of the single PZT disk, characterized as described in Section 2.1, namely the piezoelectric strain coefficient (d_{33}), the capacitance of the piezoelectric element (C_p), the relative permittivity (ε_r), and the piezoelectric voltage coefficient (g_{33}), is reported in Table 3.

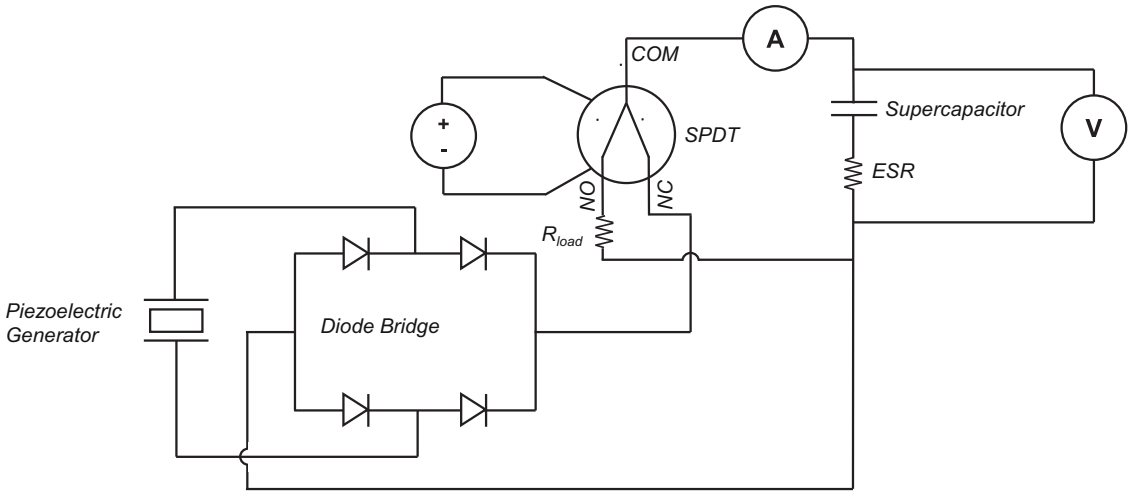

Fig. 3. Piezoelectric generator-supercapacitor coupling system.

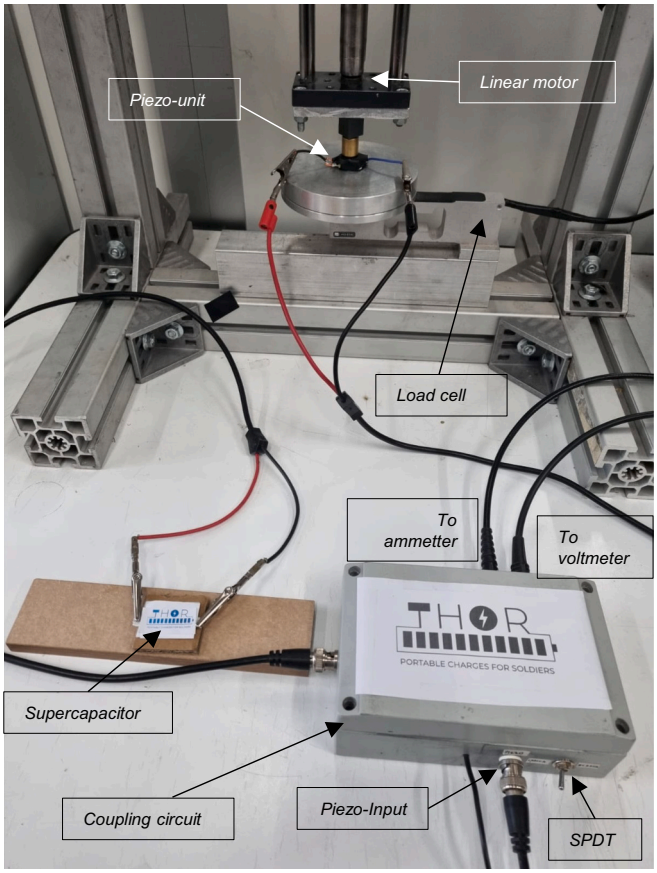

Fig. 4. Supercapacitor charging setup. The picture shows the linear motor compressing the energy harvesting unit, the coupling system (full bridge wave rectifier), and the supercapacitor.

The two different measurement techniques of the piezoelectric strain coefficient d_{33} described in Section 2.1.1 led to the same d_{33} value measured on the single PZT disk.

The energy harvesting unit described in Section 2.2 was characterized in terms of open-circuit voltage and short-circuit current (Fig. 5a and b, respectively).

Table 3
Single PZT disk characterization.

d_{33} [pC N^{-1}]	C_p [nF]	ε_r	g_{33} [mV m N^{-1}]
200	21.1	1445	15.6

The open-circuit voltage of the energy harvesting unit (blue line of Fig. 5a) presents a peak-to-peak value equal to 13.7 V and does not show a phase shift with the applied force. On the other hand, the peak-to-peak value of the short-circuit current generated by the piezoelectric unit is approximately ±120 μA. According to [37], in the case of an applied force F perpendicular to the piezoelectric specimen surface, the generated current I_p can be expressed by Eq. (7):

$$I_p = d_{33}\frac{dF}{dt} \tag{7}$$

The piezoelectric output current curve of Fig. 5b (blue line), consistently with Eq. (7), presents a derivative-like trend to the force curve (red line), with null plateau regions in correspondence with the maximum and minimum values of the applied force F. Indeed, as well known from the piezoelectric theory, the increase in the frequency of the compressive force results in higher output currents. As shown in Fig. S1, the output current of the 15 PZT-stack was measured for a frequency range of up to 20 Hz. However, with the aim to design the whole system (piezo-generator and SC) for low-frequency energy harvesting applications, the output current at 2 Hz was taken into account for the SC sizing.

3.2. Supercapacitor characteristics

At first, different sizes of SCs have been assembled to evaluate if charging currents in the order of those generated by PENG (<100 μA) enable to reach at least 3 V with a coulombic efficiency >90 %. As an example, Fig. S2 reports the GCPL charge/discharge at 50 μA of a SC featuring a footprint area of 3.8 cm^2 and a capacitance of 129 mF. Due to leakage currents that compete with the low charging one, it was not possible to overcome 3 V, and the coulombic efficiency was only 80 %. Hence, we reduced the size of the SC to 0.6 cm^2. Fig. 6a shows the schematic and an image of this SC. Fig. 6b reports the cell voltage of the 0.6 cm^2-SC under galvanostatic cycling at 50 μA and 100 μA, and room temperature. The figure demonstrates that this cell footprint enables the IL-based cell to reach voltages of 3.2 V with a coulombic efficiency >90 % even at extremely low current. Indeed, the curves in Fig. 6b feature a symmetric-triangular profile that is indicative of the reversible capacitive behavior of the device and the negligible occurrence of side reactions. Fig. S3 reports the cyclic voltammograms at different scan rates and the trends of the coulombic efficiency and capacitance over repeated galvanostatic cycles at 100 μA of the IL-pullulan-based micro-SC featuring an electrode footprint of 0.6 cm^2 and tested between 0 V and 3.2 V. The results reported in Fig. S3 demonstrate that the

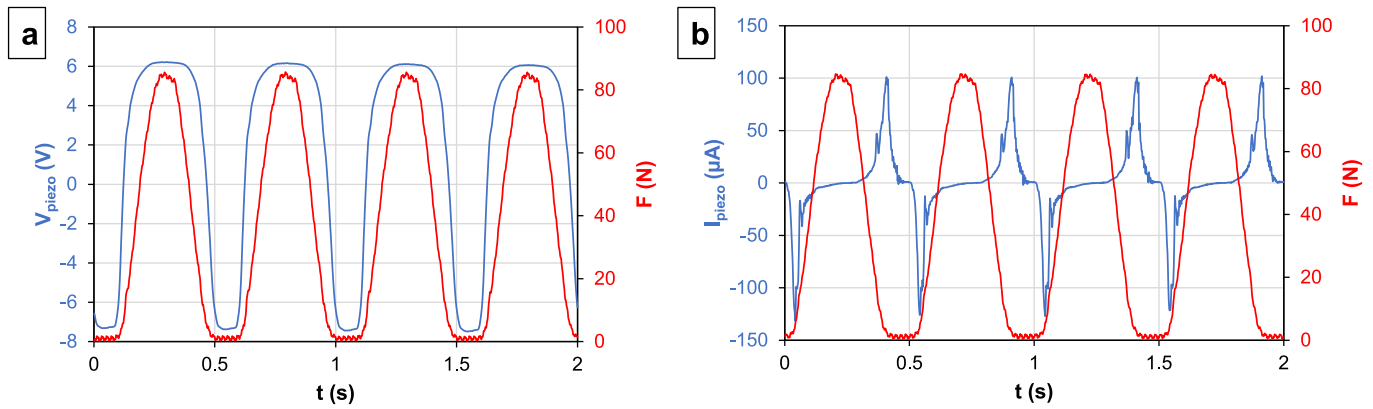

Fig. 5. (a) Open-circuit piezoelectric output voltage of the 15-PZT disks; (b) Short-circuit piezoelectric output current of the 15-PZT disks.

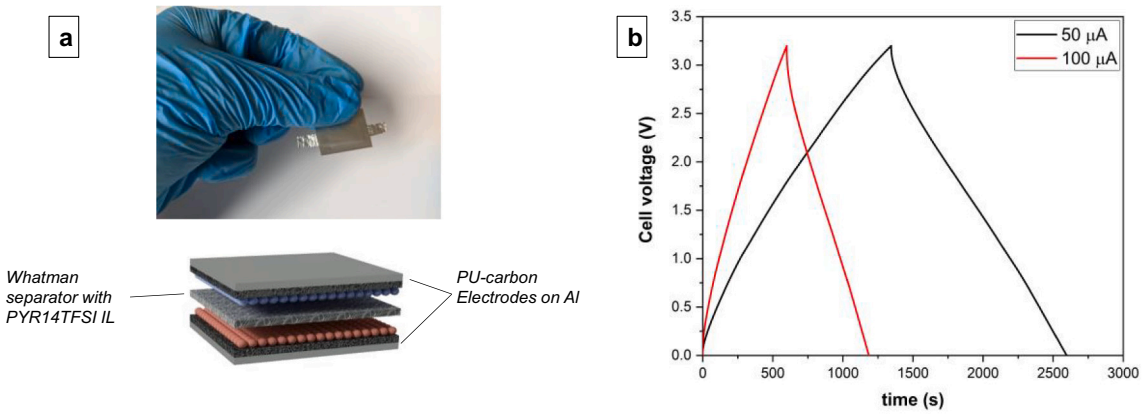

Fig. 6. a) Sketch and image of the SC and b) selected cell voltage profile under GCPL test at 50 μA and 100 μA.

combination of Pu-based electrodes and $PYR_{14}TFSI$ electrolyte enables to reach good cycling stability with cell voltage as high as 3.2 V, in agreement with refs [11–14]. Indeed, the voltammograms (Fig. S3a) maintain a symmetric, box-like shape even at a high scan rate up to 100 mV s^{-1}. At the lowest tested scan rate, the device coulombic efficiency of 99.3 %, which increased up to 99.88 % by increasing the scan rate. During the first 500 galvanostatic cycles, the cell featured good capacitance retention of c.a. 95 % with a coulombic efficiency always higher than 99 %.

Table 4 lists the characteristics of the SC. The SC capacitance (C) was ca. 22 mF and the maximum energy (Eq. (1)) resulted in ca. 100 mJ. The maximum deliverable power was calculated by taking into account an ESR of ca. 140 Ω (Eq. (4)) and resulted in 18 mW. Such value corresponds to the SC discharge through an external load having the same value of ESR. In these conditions the current I_{max} is 11.4 mA (Eq. (6)), which is >2 orders of magnitude higher than that delivered by the PENGs and used for the GCPL test.

The practical energy and power (calculated through Eqs. (1) and (5), respectively) delivered by the SC, evaluated by the analysis of the discharge profiles reported in Fig. 6b, were 92.9 mJ and 74.3 μW at 50 μA, and 83.9 mJ and 143 μW at 100 μA.

3.3. Piezo-SC charging process

The quantities measured during the charging process are the voltage of the supercapacitor (Fig. 7a), the current provided by the piezoelectric unit (Fig. 7b), and the power which is transferred from the energy harvesting unit to the supercapacitor (Fig. 7c).

As observable in Fig. 7a, the voltage charging curve follows the typical charging trend of a capacitor and after 2 h reaches a value slightly higher than 3 V. It is worth highlighting that as the linear motor applies a 2 Hz frequency sinusoidal load on the piezoelectric unit, the supercapacitor receives a 4 Hz electric signal thanks to the full-wave diode bridge rectifier. Therefore, as it can be observed in the reduced time window of Fig. 7b, the voltage charging curve of the supercapacitor shows the presence of 4 Hz-frequency peaks, whose amplitude depends on the internal resistance of the supercapacitor and the current value. The slightly higher amplitudes of the voltage peaks in the first period of the charging process are attributable to the high values of the current which passes through the internal resistance of the supercapacitor. Indeed, the amplitudes of the current peaks present a maximum value equal to 120 μA in the initial part of the process and follow a decreasing trend as the capacitor charges, before reaching a stable value of 80 μA

Table 4
Characteristics of the micro-SC evaluated by the GCPL discharge: SC capacitance, ESR, practical energy and power, maximum Energy and power, and current.

Current [μA]	Capacitance [mF]	ESR [Ω]	Coulombic efficiency η (%)	Practical energy [mJ]	Practical power [μW]	Maximum energy [mJ]	Maximum power [mW]	I_{max} [m]
50	22.6	135	91.3	92.9	74.3	102	18	11.4
100	22.4	141	97.5	83.9	143			

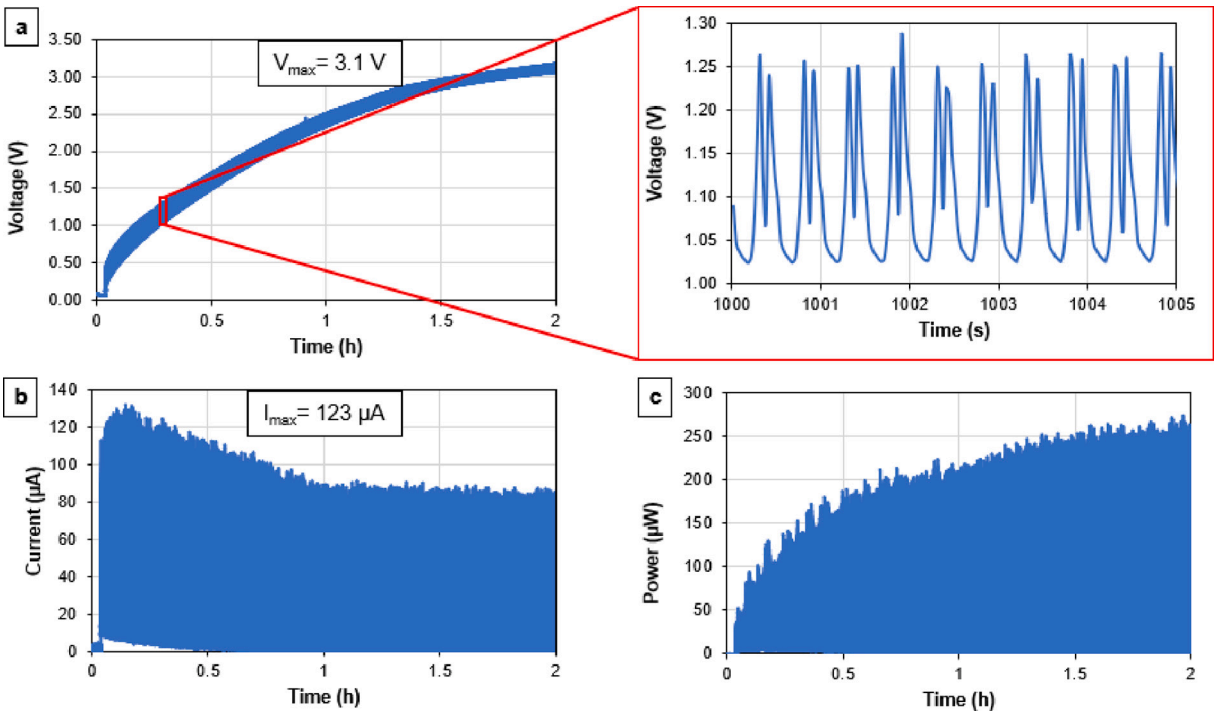

Fig. 7. (a) Charging curve of the supercapacitor during 2 h of compressive mechanical load; (b) Current provided by the piezoelectric energy harvesting unit during the charging process of the supercapacitor; (c) Instant power provided by the piezoelectric unit.

after 1 h. The power which is transferred from the piezoelectric energy harvesting unit to the supercapacitor was then calculated as $P = V \times I$, as shown in Fig. 7c. Finally, considering the final voltage of the SC equal to 3.1 V, the stored maximum energy can be simply calculated according to Eq. (1) and results equal to 110 mJ (170 mJ cm^{-2}).

3.4. Comparison of stored energy and applications

To evaluate the energy harvesting capability of the proposed system, Fig. 8 reports the values of the maximum energy stored by eSPSC and iSPSC from different works of literature. Overall, higher values are obtained in the case of using PZT as a piezoelectric generator, whose d_{33} coefficient is sensibly higher than that of PVDF and PVDF-TrFE. In addition, greater harvesting efficiencies are clearly observable when using eSPSC instead of iSPSC configuration, due to the possibility to couple the piezo-unit with the SC by using a bridge (as described in this work) which rectifies the alternate current of the piezoelectric transducer and reduces the dissipated energy. Among the proposed eSPSCs assembled with non-commercial SCs, our system stands out. It outperforms eSPSCs assembled with SCs. The advantage of our eSPSC compared to those featuring commercial button-cells is mainly the possibility of reducing the charge times and overall system volume, which is a key requisite for use in wearable devices.

As a proof of concept for a possible application, the proposed eSCSP was disconnected from the piezoelectric unit after the charging process described in Section 3.3, and it was connected to a LED, as shown in Fig. 9. The supercapacitor powered the LED for a 120 s, thus demonstrating the capability of the system to work as a power supply for low-power electronic devices. A further scale-up of the piezoelectric unit (i.e. an array of PZT stacks) and a subsequent resizing o the eSCSP could be

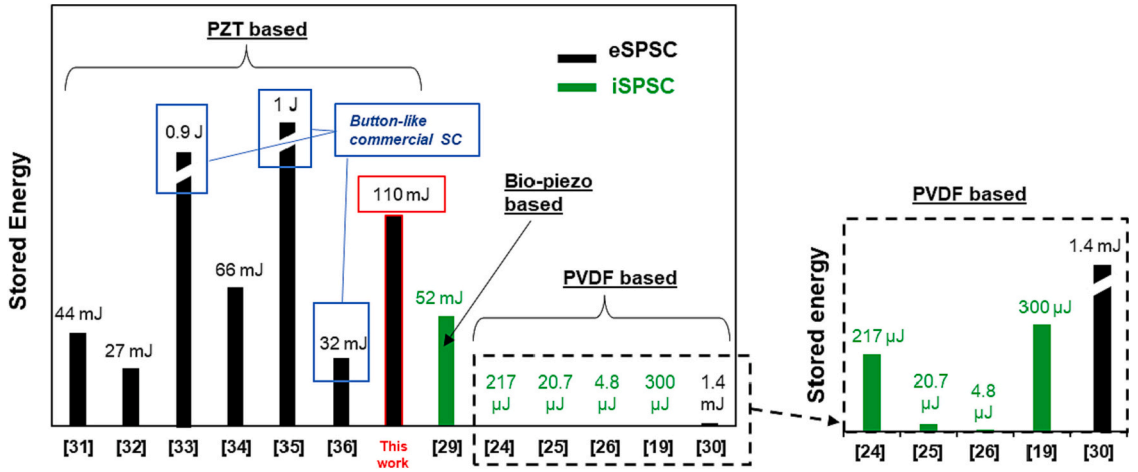

Fig. 8. Comparison between the maximum stored energy of the different works reported in literature.

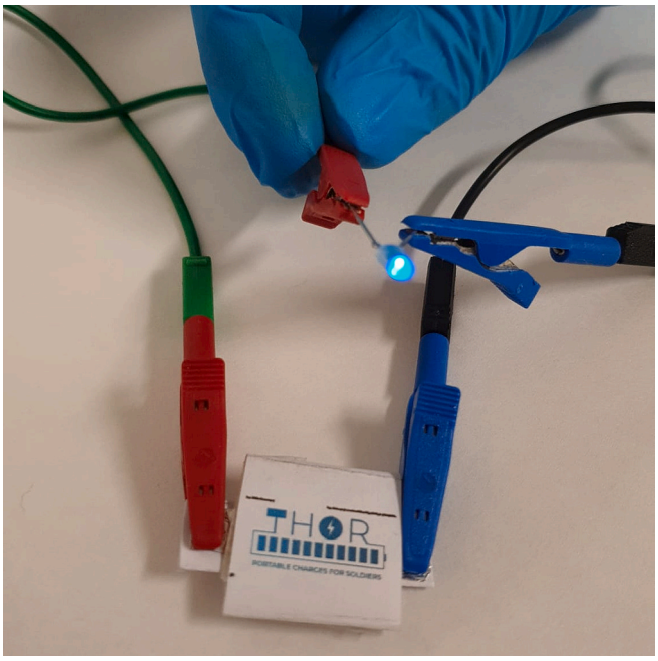

Fig. 9. Supercapacitor connected to a LED after the coupling with the piezoelectric unit.

easily performed to achieve higher powering performances for other devices, such as smart watches or phones.

4. Conclusions

A piezoelectric energy harvesting source was successfully integrated with a IL-pullulan based micro-SC. The coupling circuit comprises a full-wave bridge rectifier which converts the alternate current of the piezoelectric transducer into direct current, suitable to charge the SC. The parallel connection of the 15 PZT commercial disks provided a sufficient amount of current, which allowed to charge the properly sized SC up to 3.1 V after 2 h of compressive mechanical stimuli of 85 N at 2 Hz. Multiple charge/discharge tests were performed in the same test conditions without any visible damage to the SC structure and the results were consistent. As a proof of concept for a possible application, the SC was successfully used to light a LED for 120 s. The two units-based system (piezo-generator and supercapacitor) enables an appropriate sizing of the micro-SC according to the output current of the PZT stack. Higher performances can be achieved with a multiple connection of the PZT stack in an array-like disposition which enhances the stored energy in the tailored micro-SC. Overall, our integrated system is capable to store up to 110 mJ in 2 h, therefore outperforming the energy characteristics of SPSC assembled with micros-SC (both iSPSC and eSPSC) with charge times shorter than those demonstrated using commercial SCs.

CRediT authorship contribution statement

Giacomo Selleri, Federico Poli, Riccardo Neri, Leonardo Gasperini: Conceptualization, Methodology, Investigation, Formal analysis, Writing – original draft. Francesca Soavi, Chiara Gualandi, Davide Fabiani: Investigation, Supervision, Conceptualization, and Review editing.

Declaration of competing interest

The authors declare that they have no known competing financial interests or personal relationships that could have appeared to influence the work reported in this paper.

Data availability

Data will be made available on request.

Acknowledgments

This work was supported by THOR - lighTweight self-cHarging piezO-supercapacitoR systems by nanotechnologies (Portable Charges for Soldiers) - NATO Science for Peace and Security Programme, under grant agreement G5772.

Appendix A. Supplementary data

Supplementary data to this article can be found online at https://doi.org/10.1016/j.est.2023.106660.

References

[1] M. Prauzek, J. Konecny, M. Borova, K. Janosova, J. Hlavica, P. Musilek, Energy harvesting sources, storage devices and system topologies for environmental wireless sensor networks: a review, Sensors (Switzerland) 18 (8) (2018) pp, https://doi.org/10.3390/s18082446.
[2] N. Sezer, M. Koç, A comprehensive review on the state-of-the-art of piezoelectric energy harvesting, Nano Energy 80 (November 2020) (2021), 105567, https://doi.org/10.1016/j.nanoen.2020.105567.
[3] C. Chen, T.B. Xu, A. Yazdani, J.Q. Sun, A high density piezoelectric energy harvesting device from highway traffic — system design and road test, Appl. Energy 299 (June) (2021), 117331, https://doi.org/10.1016/j.apenergy.2021.117331.
[4] J. Briscoe, S. Dunn, Piezoelectric nanogenerators - a review of nanostructured piezoelectric energy harvesters, Nano Energy 14 (2014) 15–29, https://doi.org/10.1016/j.nanoen.2014.11.059.
[5] Y. Sugawara, K. Onitsuka, S. Yoshikawa, Q. Xu, R.E. Newnham, K. Uchino, Metal–Ceramic composite actuators, J. Am. Ceram. Soc. 75 (4) (1992) 996–998, https://doi.org/10.1111/j.1151-2916.1992.tb04172.x.
[6] D. Arnold, W. Kinsel, W.W. Clark, C. Mo, Exploration of new cymbal design in energy harvesting, Act. Passiv. Smart Struct. Integr. Syst. 7977 (March) (2011) 79770T, https://doi.org/10.1117/12.880614, 2011.
[7] D. Motter, J.V. Lavarda, F.A. Dias, S. da Silva, Vibration energy harvesting using piezoelectric transducer and non-controlled rectifiers circuits, J. Brazilian Soc. Mech. Sci. Eng. 34 (spe) (2012) 378–385, https://doi.org/10.1590/s1678-58782012000500006.
[8] F. Soavi, et al., Miniaturized supercapacitors: key materials and structures towards autonomous and sustainable devices and systems, J. Power Sources 326 (2016) 717–725, https://doi.org/10.1016/j.jpowsour.2016.04.131.
[9] L. Naderi, S. Shahrokhian, F. Soavi, Fabrication of a 2.8 v high-performance aqueous flexible fiber-shaped asymmetric micro-supercapacitor based on MnO2/PEDOT:PSS-reduced graphene oxide nanocomposite grown on carbon fiber electrode, J. Mater. Chem. A 8 (37) (2020) 19588–19602, https://doi.org/10.1039/d0ta06561g.
[10] G. Wu, S. Sun, X. Zhu, Z. Ma, Y. Zhang, N. Bao, Microfluidic fabrication of hierarchical-ordered ZIF-L(Zn)@Ti3C2Tx Core-sheath fibers for high-performance asymmetric supercapacitors, Angew. Chemie Int. Ed. 61 (8) (2022), e202115559, https://doi.org/10.1002/anie.202115559.
[11] G.E. Spina, F. Poli, A. Brilloni, D. Marchese, F. Soavi, Natural polymers for green supercapacitors, Energies 13 (12) (2020), https://doi.org/10.3390/en13123115.
[12] F. Poli, et al., Pullulan-ionic liquid-based supercapacitor: a novel, smart combination of components for an easy-to-dispose device, Electrochim. Acta 338 (2020), 135872, https://doi.org/10.1016/j.electacta.2020.135872.
[13] A. Brilloni, et al., Easy recovery of li-ion cathode powders by the use of water-processable binders, Electrochim. Acta 418 (April) (2022), 140376, https://doi.org/10.1016/j.electacta.2022.140376.
[14] A. Brilloni, F. Marchesini, F. Poli, E. Petri, F. Soavi, Performance comparison of LMNO cathodes produced with pullulan or PEDOT:PSS water-processable binders, Energies 15 (7) (2022) pp, https://doi.org/10.3390/en15072608.
[15] B.K. Udaya, D.B. Panemangalore, Ionic Liquid Electrolytes for Flexible Supercapacitors, 2021.
[16] L.G. Bettini, P. Piseri, F. De Giorgio, C. Arbizzani, P. Milani, F. Soavi, Flexible, ionic liquid-based micro-supercapacitor produced by supersonic cluster beam deposition, Electrochim. Acta 170 (2015) 57–62, https://doi.org/10.1016/j.electacta.2015.04.068.
[17] F. Soavi, C. Arbizzani, M. Mastragostino, Leakage currents and self-discharge of ionic liquid-based supercapacitors, J. Appl. Electrochem. 44 (4) (2014) 491–496, https://doi.org/10.1007/s10800-013-0647-x.
[18] R. Kötz, M. Hahn, R. Gallay, Temperature behavior and impedance fundamentals of supercapacitors, J. Power Sources 154 (2) (2006) 550–555, https://doi.org/10.1016/j.jpowsour.2005.10.048.
[19] C. Rokaya, P. Schaeffner, S. Tuukkanen, J. Keskinen, D. Lupo, Motion energy harvesting and storage system including printed piezoelectric film and supercapacitor, IEEE Int. Flex. Electron. Technol. Conf. IFETC 2019 (2019), https://doi.org/10.1109/IFETC46817.2019.9073717.

[20] B. Singh, B. Padha, S. Verma, S. Satapathi, V. Gupta, S. Arya, Recent advances, challenges, and prospects of piezoelectric materials for self-charging supercapacitor, J. Energy Storage 47 (July) (2021) 2022, https://doi.org/10.1016/j.est.2021.103547.
[21] X. Pu, W. Hu, Z.L. Wang, Toward wearable self-charging power systems: the integration of energy-harvesting and storage devices, Small 14 (1) (2018) 1–19, https://doi.org/10.1002/smll.201702817.
[22] M.H. Chung, et al., Enhanced output performance on LbL multilayer PVDF-TrFE piezoelectric films for charging supercapacitor, Sci. Rep. 9 (1) (2019) 6–11, https://doi.org/10.1038/s41598-019-43098-6.
[23] A. Ramadoss, B. Saravanakumar, S.W. Lee, Y.S. Kim, S.J. Kim, Z.L. Wang, Piezoelectric-driven self-charging supercapacitor power cell, ACS Nano 9 (4) (2015) 4337–4345, https://doi.org/10.1021/acsnano.5b00759.
[24] R. Song, et al., A rectification-free piezo-supercapacitor with a polyvinylidene fluoride separator and functionalized carbon cloth electrodes, J. Mater. Chem. A 3 (29) (2015) 14963–14970, https://doi.org/10.1039/c5ta03349g.
[25] Y. Lu, Y. Jiang, Z. Lou, R. Shi, D. Chen, G. Shen, Wearable supercapacitor self-charged by P(VDF-TrFE) piezoelectric separator, Prog. Nat. Sci. Mater. Int. 30 (2) (2020) 174–179, https://doi.org/10.1016/j.pnsc.2020.01.023.
[26] K. Parida, V. Bhavanasi, V. Kumar, J. Wang, P.S. Lee, Fast charging self-powered electric double layer capacitor, J. Power Sources 342 (2017) 70–78, https://doi.org/10.1016/j.jpowsour.2016.11.083.
[27] E.P. Gilshteyn, et al., Flexible self-powered piezo-supercapacitor system for wearable electronics, Nanotechnology 29 (32) (2018), https://doi.org/10.1088/1361-6528/aac658.
[28] K. Krishnamoorthy, P. Pazhamalai, V.K. Mariappan, S.S. Nardekar, S. Sahoo, S. J. Kim, Probing the energy conversion process in piezoelectric-driven electrochemical self-charging supercapacitor power cell using piezoelectrochemical spectroscopy, Nat. Commun. 11 (1) (2020) 1–11, https://doi.org/10.1038/s41467-020-15808-6.
[29] A. Maitra, et al., Fast charging self-powered wearable and flexible asymmetric supercapacitor power cell with fish swim bladder as an efficient natural bio-piezoelectric separator, Nano Energy 40 (August) (2017) 633–645, https://doi.org/10.1016/j.nanoen.2017.08.057.
[30] Z. He, et al., Piezoelectric-driven self-powered patterned electrochromic supercapacitor for human motion energy harvesting, ACS Sustain. Chem. Eng. 7 (1) (2019) 1745–1752, https://doi.org/10.1021/acssuschemeng.8b05606.
[31] G.T. Hwang, et al., Self-powered wireless sensor node enabled by an aerosol-deposited PZT flexible energy harvester, Adv. Energy Mater. 6 (13) (2016) 1–9, https://doi.org/10.1002/aenm.201600237.
[32] L. Yuan, et al., Paper-based supercapacitors for self-powered nanosystems, Angew. Chemie - Int. Ed. 51 (20) (2012) 4934–4938, https://doi.org/10.1002/anie.201109142.
[33] M.F. Mahmood, S.L. Mohammed, S.K. Gharghan, Energy harvesting-based vibration sensor for medical electromyography device, Int. J. Electr. Electron. Eng. Telecommun. 9 (5) (2020) 364–372, https://doi.org/10.18178/ijeetc.9.5.364-372.
[34] T.B. Xu, et al., Energy harvesting using a PZT ceramic multilayer stack, Smart Mater. Struct. 22 (6) (2013) pp, https://doi.org/10.1088/0964-1726/22/6/065015.
[35] Y. Ma, Q. Ji, S. Chen, G. Song, An experimental study of ultra-low power wireless sensor-based autonomous energy harvesting system, J. Renew. Sustain. Energy 9 (5) (2017) pp, https://doi.org/10.1063/1.4997274.
[36] M. Sofwan, M. Resali, Development of multiple-input power management circuit for piezoelectric harvester, J. Mech. Eng. 2 (2) (2017) 215–230.
[37] M. Serridge, T.R. Licht [Online]. Available, in: Accelerometers Piezoelectric and Vibration Preamplifiers. Theory and Application Handbook, 1987, p. 151, http://www.bksv.com/Products/transducers/vibration/accelerometers/handbook.aspx.